# Conductive surface oxide on CrN(001) layers

Mary E. McGahay and Daniel Gall\*

Department of Materials Science and Engineering, Rensselaer Polytechnic Institute, Troy, NY 12180, USA

### **Abstract**

Epitaxial CrN(001) layers that are exposed to an O<sub>2</sub>-containing atmosphere exhibit a conductive 2D surface oxide with a sheet conductance  $G_{s,oxide} = 5.9 \times 10^{-5} [\Omega/\Box]^{-1}$ . This is demonstrated using *in situ* transport measurements in a 90% Ar - 10% O<sub>2</sub> mixture with continuously increasing pressure from <10<sup>-6</sup> to 240 Pa, showing a conductance increase that is independent of the CrN thickness d = 10 and 300 nm but is absent for control samples that are capped with insulating AlN prior to oxygen exposure. This suggests n-type doping of semiconducting CrN through substitutional replacement of N surface atoms with O. Cooling to 77 K leads to a decrease in  $G_{s,oxide}$  to  $3.9 \times 10^{-5} [\Omega/\Box]^{-1}$ , indicating that the conduction electrons are not fully delocalized. The overall results indicate a path towards 2D electron transport devices in refractory transition metal nitrides and may explain the large variation in previously reported transport properties of CrN.

### Main text

Chromium nitride has gained considerable interest because of its magnetic ordering and possible band gap<sup>1-4</sup> that make it a promising material for dilute magnetic semiconductors, especially when combined with other nitride semiconductors.<sup>5-7</sup> In addition, CrN also shows promise as a thermoelectric material<sup>8-10</sup> and is widely used as an oxidation and wear resistant layer in protective 9-11 and self-lubricious hard-coatings. 14-17 No consensus has been reached regarding the electronic transport properties in CrN. Reported values for the room-temperature resistivity  $\rho$  range over five orders of magnitude, from  $3\times10^{-4}$  to  $20~\Omega$ -cm<sup>1,2,5,17-29</sup> with the most reliable data for single crystal layers within the narrower range of  $8.2 \times 10^{-3}$ - $1.7 \times 10^{-1}$   $\Omega$ -cm. <sup>1,2,5,21</sup>-<sup>23,26-29</sup> Even more controversial is the temperature dependence of  $\rho$ . Some studies report metallic behavior<sup>22-24</sup> with a positive  $d\rho/dT$ , while others measure a decreasing  $\rho$  with increasing temperature, 1,5,7,21,27-29 which is attributed to a band gap 1,21 or weak carrier localization due to N vacancies<sup>8</sup> or crystalline defects.<sup>25</sup> Additionally, some studies report a discontinuity in  $\rho(T)$ between 260-280 K, 5,8,22,23 which is associated with a magnetic and structural phase transition from a paramagnetic cubic NaCl structure at room temperature to a low-temperature antiferromagnetic orthorhombic P<sub>nma</sub> phase<sup>24</sup> with a 0.56%-0.59% higher density<sup>24</sup> and a 25% lower bulk modulus.<sup>30</sup> Some studies suggest that CrN transport properties may be strongly affected by deposition conditions including temperature, <sup>29</sup> N<sub>2</sub> partial pressure, <sup>31</sup> and the substrate type, <sup>28,30</sup> and that small concentrations of oxygen impurities may increase its conductivity <sup>32,33</sup> while larger concentrations lead to insulating CrO<sub>x</sub>N<sub>y</sub> films with resistivities that are several orders of magnitude higher than that of stoichiometric CrN films. 33-35 These latter results suggest

<sup>\*</sup> Email: galld@rpi.edu

that understanding the effect of oxygen exposure may be the key to resolve the controversy about CrN transport properties.

In this letter, we demonstrate a dramatic resistivity decrease during room-temperature oxygen exposure of epitaxial CrN(001) layers. This result is initially surprising, considering that CrN is used as a high-temperature oxidation-resistant coating and that room-temperature oxidation results in a native oxide < 1 nm thick. <sup>36-39</sup> In situ transport measurements during oxygen exposure indicate the formation of a 2D conductive surface layer with a sheet conductance that is independent of the CrN layer thickness. This conductive layer may be attributed to nitrogen-to-oxygen substitutions at the surface which are expected to cause n-type doping. The overall results may explain the reported controversial CrN transport properties and also indicate a path towards devices based on 2D electron transport in refractory transition metal nitrides.

The epitaxial CrN(001) layers, 10 and 300 nm thick, were grown in a three-chamber ultrahigh vacuum DC magnetron sputtering system with a base pressure of 10<sup>-7</sup> Pa and in situ transport measurement capabilities, as described in Refs. 40 and 41. Prior to deposition, singleside polished 10×10×0.5 mm<sup>3</sup> MgO(001) wafers were cleaned with successive rinses in ultrasonic baths of tri-chloroethylene, acetone, isopropyl alcohol, and de-ionized water, inserted into the deposition system and thermally degassed in vacuum at 1000 °C for one hour. Subsequently, the substrate temperature was lowered to 750 °C, a 5-cm-diameter 99.95% pure Cr target was positioned 10.5 cm from the substrate at an angle of 45°, and a processing gas pressure of 0.4 Pa was reached with a constant flux of 99.999% pure N<sub>2</sub> that was further purified with a MicroTorr purifier yielding a nominal O<sub>2</sub> impurity content <10<sup>-9</sup>. A constant power of 350 W was applied to the magnetron, yielding a growth rate of 15 nm/min, as determined from thickness measurements by x-ray reflectivity. These deposition conditions are expected to yield stoichiometric compositions with a N:Cr ratio of 1.00±0.06<sup>1,26,29</sup> and to form epitaxial CrN(001) layers.  $^{26,42,43}$  The latter is confirmed using a combination of x-ray diffraction  $\theta$ -2 $\theta$  scans,  $\omega$ rocking curves,  $\varphi$ -scans, and reciprocal space maps similar to those in Refs. 1,26, 44, 45, which show that all CrN layers in our study are epitaxial single-crystals. After deposition, the samples were allowed to cool to room temperature (295±1 K), followed by transport without breaking vacuum to an adjacent analysis chamber with a base pressure of 10<sup>-7</sup> Pa. Electron transport properties were measured using an *in situ* linear four-point probe with spring-loaded tips with 1mm inter-probe spacings, a Keithley 2182A Nanovoltmeter and a Keithley 6220 Precision Current Source providing 1.00 µA.

Figure 1 shows the measured sheet conductance  $G_s$  of epitaxial CrN(001) layers during room-temperature oxygen exposure experiments. For this purpose, a constant flux of a 90% Ar-10%  $O_2$  mixture is introduced to the analysis chamber through a needle valve, leading to a linearly increasing pressure with dp/dt = 0.053 Pa/s. Simultaneously, the sheet conductance is measured continuously over an oxidation time  $t_{ox} = 0 - 4480$  s, corresponding to a pressure increase from  $10^{-6}$  to 240 Pa. That is, the  $O_2$  partial pressure increases linearly from zero to 24 Pa during the 4480 s of the oxidation experiment. Fig. 1(a) shows the  $G_s$  from a 10-nm-thick CrN(001) layer during such an oxidation experiment, plotted vs  $t_{ox}$  in a logarithmic scale. The top x-axis indicates the corresponding  $O_2$  exposure, which is the time-integral over the oxygen partial pressure. Prior to gas introduction ( $t_{ox} \le 0$  s), the sheet conductance is  $0.18 \times 10^{-4} [\Omega/\Box]^{-1}$ . It continuously increases with  $t_{ox} > 0$  s to  $0.24 \times 10^{-4} [\Omega/\Box]^{-1}$  for  $t_{ox} = 10$  s,  $0.69 \times 10^{-4} [\Omega/\Box]^{-1}$  for  $t_{ox} = 10$  s,  $0.69 \times 10^{-4} [\Omega/\Box]^{-1}$  for  $t_{ox} = 10$  s,  $0.69 \times 10^{-4} [\Omega/\Box]^{-1}$  for  $t_{ox} = 10$  s,  $0.69 \times 10^{-4} [\Omega/\Box]^{-1}$  for  $t_{ox} = 10$  s,  $0.69 \times 10^{-4} [\Omega/\Box]^{-1}$  for  $t_{ox} = 10$  s,  $0.69 \times 10^{-4} [\Omega/\Box]^{-1}$  for  $t_{ox} = 10$  s,  $0.69 \times 10^{-4} [\Omega/\Box]^{-1}$  for  $t_{ox} = 10$  s,  $0.69 \times 10^{-4} [\Omega/\Box]^{-1}$  for  $t_{ox} = 10$  s,  $0.69 \times 10^{-4} [\Omega/\Box]^{-1}$  for  $t_{ox} = 10$  s,  $0.69 \times 10^{-4} [\Omega/\Box]^{-1}$  for  $t_{ox} = 10$  s,  $0.69 \times 10^{-4} [\Omega/\Box]^{-1}$  for  $t_{ox} = 10$  s,  $0.69 \times 10^{-4} [\Omega/\Box]^{-1}$  for  $t_{ox} = 10$  s,  $0.69 \times 10^{-4} [\Omega/\Box]^{-1}$  for  $t_{ox} = 10$  s,  $0.69 \times 10^{-4} [\Omega/\Box]^{-1}$  for  $t_{ox} = 10$  s,  $0.69 \times 10^{-4} [\Omega/\Box]^{-1}$  for  $t_{ox} = 10$  s,  $0.69 \times 10^{-4} [\Omega/\Box]^{-1}$  for  $t_{ox} = 10$  s,  $0.69 \times 10^{-4} [\Omega/\Box]^{-1}$ 

100 s, and  $0.75 \times 10^{-4} \, [\Omega/\Box]^{-1}$  for  $t_{ox} = 1000$  s, reaching an approximately constant  $G_s = 0.76 \times 10^{-4} \, [\Omega/\Box]^{-1}$  when the experiment is terminated after 4480 s. The majority of the conductance increase occurs within a relatively narrow time interval of  $t_{ox} = 25$ -40 s, where the plotted curve shows a steep increase. We note that this is not just an artifact of the plotted logarithmic scale, but that the  $G_s$  vs  $t_{ox}$  curve also exhibits regions of positive curvature when plotted linearly (not shown), and that there is a maximum in the derivative  $dG_s/dt_{ox} = 3 \times 10^{-6} \, [\Omega/\Box]^{-1}/s$  at  $t_{ox} = 32$  s. We also note that the apparent slope for  $t_{ox} < 1$  s in Fig. 1(a), may be an artifact of the logarithmic scale in combination with the uncertainty of  $\pm 1$  s in the exact starting time, while the data gap between  $t_{ox} = 880$  and 1280 s is due to a data requisition software error.

The plot in Fig. 1(b) shows the measured  $G_s$  vs  $t_{ox}$  from a CrN(001) layer with thickness d=300 nm. Its sheet conductance prior to oxygen exposure is  $4.3 \times 10^{-4} [\Omega/\Box]^{-1}$ . This value is 20 times larger than for d=10 nm, which is attributed to the 30 times larger thickness and indicates approximately linear scaling of the conductance, as expected. The plotted curve is qualitatively similar to that shown in Fig. 1(a), exhibiting the largest increase in  $G_s$  from  $4.3 \times 10^{-4}$  to  $4.7 \times 10^{-4}$   $[\Omega/\Box]^{-1}$  between  $t_{ox}=30$ -50 s, followed by a more gradual increase to  $4.9 \times 10^{-4} [\Omega/\Box]^{-1}$  for  $t_{ox}=4480$  s. This latter value is retained when removing the sample from the vacuum system and exposing it to atmospheric air, as indicated by the data point plotted in Fig. 1(b) for an exposure of  $10^7$  Pa-s, corresponding to an air exposure of approximately 10 minutes and an *ex situ* measured  $G_s=4.9 \times 10^{-4} [\Omega/\Box]^{-1}$ .

Figure 1(b) also shows the measured  $G_s$  (purple line) from a second 300-nm-thick CrN(001) layer that is deposited at identical conditions as the first layer (red line), however, immediately after CrN deposition, this second layer was capped with a 4-nm-thick AlN layer using pulsed reactive DC sputtering from a 99.99% pure Al target at 750 °C. This AlN layer is expected to be insulating and therefore to not affect the measured  $G_s$ , but to protect the underlying CrN from oxygen exposure. The measured sheet resistance of this capped CrN layer prior to oxygen exposure is  $4.2\times10^{-4}$  [ $\Omega/\Box$ ]<sup>-1</sup>, which is within 2% of the first CrN layer, indicating good sample to sample reproducibility from two nominally identical 300-nm-thick CrN(001) layers. The measured  $G_s$  remains constant within experimental uncertainty for  $t_{ox}$ 100 s and subsequently decreases slightly (by 2%) to a value of  $4.1 \times 10^{-4} [\Omega/\Box]^{-1}$  which is unaffected by further air exposure. The exact reasons for the observed modest decrease in  $G_s$  are not known, but may be attributed to a 0.5 K temperature decrease during the ~1 hour exposure to an increasing gas pressure, as estimated using the temperature coefficient of resistivity (TCR) of -1.7×10<sup>-3</sup> Ω-cm/K measured ex situ between 7 and 20 °C. This TCR value is within the large range of previously reported values,  $-2 \times 10^{-5}$  to  $-5 \times 10^{-3}$   $\Omega$ -cm/K, from epitaxial CrN layers at temperatures near room temperature. <sup>26-29</sup> Independent of this minor detail, the CrN layer that is capped with AlN clearly does not exhibit the strong increase in  $G_s$  that is recorded for the pristine CrN(001) layer, suggesting that this increase is associated with O<sub>2</sub> exposure of the pristine CrN surface.

After the *in situ* oxygen exposure experiments, the samples are removed from the vacuum system through a load-lock that is filled with dry N<sub>2</sub>, and immediately dropped into liquid N<sub>2</sub> for transport measurements with both sample and probe tips submerged in liquid N<sub>2</sub>. This yields values for the sheet conductance at 77 K of  $G_s = 3.9 \times 10^{-5}$ ,  $5.4 \times 10^{-5}$ , and  $1.5 \times 10^{-5}$  [ $\Omega/\Box$ ]<sup>-1</sup> for the three samples presented in Fig. 1, namely for d = 10 nm and d = 300 nm without and with AlN cap, respectively. These values are also listed in Table I. All three samples exhibit a decrease in

the conductance with decreasing temperature, indicating carrier localization. This is consistent with previous reports of a negative  $TCR^{5,21,27-29}$  and variable range hopping at low temperatures<sup>21,29</sup> while, however, some studies also report a positive TCR for CrN.<sup>22-24</sup> The conductance of the AlN-capped layer can be used to directly determine the CrN resistivity, because it is not affected by the confounding conductance of the surface oxide. Thus, we find  $\rho_{295K} = 7.1 \times 10^{-2} \Omega$ -cm and  $\rho_{77K} = 2.0 \Omega$ -cm at room temperature and liquid N<sub>2</sub>, respectively. These values are within the ranges of previously reported values from epitaxial layers,  $8.2 \times 10^{-3}$ - $1.7 \times 10^{-1} \Omega$ -cm at room temperature,  $^{1,2,5,21-23,26-29}$  and  $1 \times 10^{-2}$  - 5  $\Omega$ -cm at 77 K for layers with a negative TCR.<sup>21,28,29</sup> After the measurements at 77 K, the samples were warmed up to room temperature (295±1 K) by blowing dry N<sub>2</sub> gas onto their surface, followed by *ex situ* measurements in air, as also plotted in Fig. 1 and discussed above.

Table I lists the measured  $G_s$  of the as-deposited and air-exposed layers, as well as the increase  $\Delta G_s$  during oxygen exposure, that is, the difference between the air-exposed and the asdeposited values. They are  $\Delta G_s = 0.58 \times 10^{-4}$  and  $0.60 \times 10^{-4}$  [ $\Omega/\Box$ ]<sup>-1</sup> for the 10 and 300 nm thick CrN(001) layers, respectively. The two values of  $\Delta G_s$  are nearly identical, suggesting that the increase in conductance for the 10 and 300 nm thick layers are due to the same physical process, which we postulate to be the formation of a conductive surface oxide with a sheet conductance of  $G_{s,oxide} = 5.9 \pm 0.2 \times 10^{-5} [\Omega/\Box]^{-1}$  from the average of the two measured values. The thickness independence of  $\Delta G_s$  suggests that the conductive oxide does not replace a considerable fraction of the (less-conducting) original CrN layer, consistent with the known high oxidation-resistance of CrN. 36-39 Therefore, we expect the surface oxide to be thin, possibly only a monolayer thick and definitely below 2 nm, yielding an upper bound for its resistivity  $\leq 3 \times 10^{-3} \ \Omega \text{cm}$ . The AlNcapped layer has a small and negative  $\Delta G_s = -9 \times 10^{-6} \ [\Omega/\Box]^{-1}$ , confirming that the AlN layer impedes the formation of the conductive oxide layer, while the slight negative value may be due to a 0.5 K variation in T, as discussed above. We note that the relative uncertainty is approximately 2% for both  $G_s$  and  $\Delta G_s$ , such that the absolute experimental uncertainty in the measured  $\Delta G_s$  is smaller than in  $G_s$ , particularly for the 300-nm-thick layers. This is because  $\Delta G_s$ is measured in a single oxygen exposure experiment which does not require repositioning of the 4-point-probe. The latter is the primary source of uncertainty due to the related geometrical correction factors.

We now quantitatively discuss the low-temperature (77 K) data by comparing the measured  $G_s$  from the different samples. Similar to above, we describe the sheet conductance of the air-exposed layers as the sum of  $G_s$  of the CrN layer plus  $G_s$  of the surface oxide, while the AlN-capped layer conducts only within the CrN. Correspondingly, we directly determine the CrN resistivity at 77 K from  $G_s = 1.5 \times 10^{-5} [\Omega/\Box]^{-1}$  of the 300-nm-thick capped layer to be  $\rho_{77K} = 2.0 \ \Omega$ -cm. The difference between the conductance of the air-exposed and capped CrN corresponds to the conductance of the surface oxide. Thus, we determine  $G_{s,oxide} = 3.9 \times 10^{-5} [\Omega/\Box]^{-1}$  for the surface oxide at 77 K from the difference between  $5.4 \times 10^{-5}$  and  $1.5 \times 10^{-5} [\Omega/\Box]^{-1}$  from the 300-nm-thick pristine and AlN-capped layers, respectively. Now, we evaluate if these results are consistent with the measured  $G_s$  of the 10-nm-thick layer at 77 K. For this purpose we estimate the expected sheet conductance for the 10-nm-thick layer as the sum of  $G_{s,oxide} = 3.9 \times 10^{-5} [\Omega/\Box]^{-1}$  (from above) plus the CrN sheet conductance which is  $d/\rho_{77K} = 10 \text{ nm} / 2.0 \ \Omega$ -cm =  $0.05 \times 10^{-5} [\Omega/\Box]^{-1}$ . Thus, based on the data from the 300-nm-thick layers, we expect the 10-nm-layer to have a 77 K sheet conductance of  $3.9 \times 10^{-5} + 0.05 \times 10^{-5} = 3.9(5) \times 10^{-5} [\Omega/\Box]^{-1}$ , which

is in perfect agreement with the directly measured  $3.9 \times 10^{-5} [\Omega/\Box]^{-1}$ . This also shows that the conductance of the surface oxide completely dominates transport in the d = 10 nm layer at 77 K.

In conclusion, in situ oxygen exposure experiments on three CrN samples indicate the formation of a conductive surface oxide with a sheet conductance  $G_{s,oxide} = 5.9 \times 10^{-5}$  and  $3.9 \times 10^{-5}$  $[\Omega/\Box]^{-1}$  at 295 and 77 K, respectively. We attribute the conductive oxide surface layer to substitutional replacement of N with O atoms, which are expected to act as n-type dopants that yield localized states near the conduction band which, at a critical concentration, result in a transition from insulating CrN to conductive CrN<sub>1-x</sub>O<sub>x</sub> and cause a relatively abrupt increase in the measured  $G_s$  during our oxidation experiments. However, we note that chromium-oxynitride layers with considerable oxygen concentrations have been reported to be insulators, 33-35 which can be attributed to an increasing electron correlation and associated electron localization with increasing oxygen content, while moderate oxygen-doping of CrN increases the conductivity. 32,33 We also note that we do not expect the surface oxide to consist of the half-metallic CrO<sub>2</sub> phase, <sup>46</sup> which typically forms by decomposition from CrO<sub>3</sub> but has never been reported to develop during CrN oxidation.  $^{36-39}$  The decrease in  $G_{s,oxide}$  with decreasing T indicates that the dopant electrons are not fully delocalized, despite that the surface oxide is more than an order of magnitude more conductive than the CrN. This dramatic difference may explain some of the contradicting reports on electron transport in CrN and promises possible 2D electron transport devices on transition metal nitride surfaces.

## Acknowledgements

The authors acknowledge financial support by the National Science Foundation under Grant Nos. 1712752, 1537984, and 1629230.

d (nm)	$G_s \left(10^{-4} \left[\Omega/\Box\right]^{-1}\right)$			
	As-deposited, 295 K	Air-exposed, 295 K	Air-exposed, 77 K	$\Delta G_s$
10	0.18	0.76	0.39	0.58
300	4.3	4.9	0.54	0.60
300 with AlN cap	4.2	4.1	0.15	-0.09

Table I: Sheet conductance  $G_s$  measured in situ at 295 K, ex situ at 295 K, and immersed in liquid nitrogen at 77 K of CrN(001) layers with thickness d = 10 nm, 300 nm, and 300 nm capped with AlN.  $\Delta G_s$  is the change in  $G_s$  during oxygen exposure.

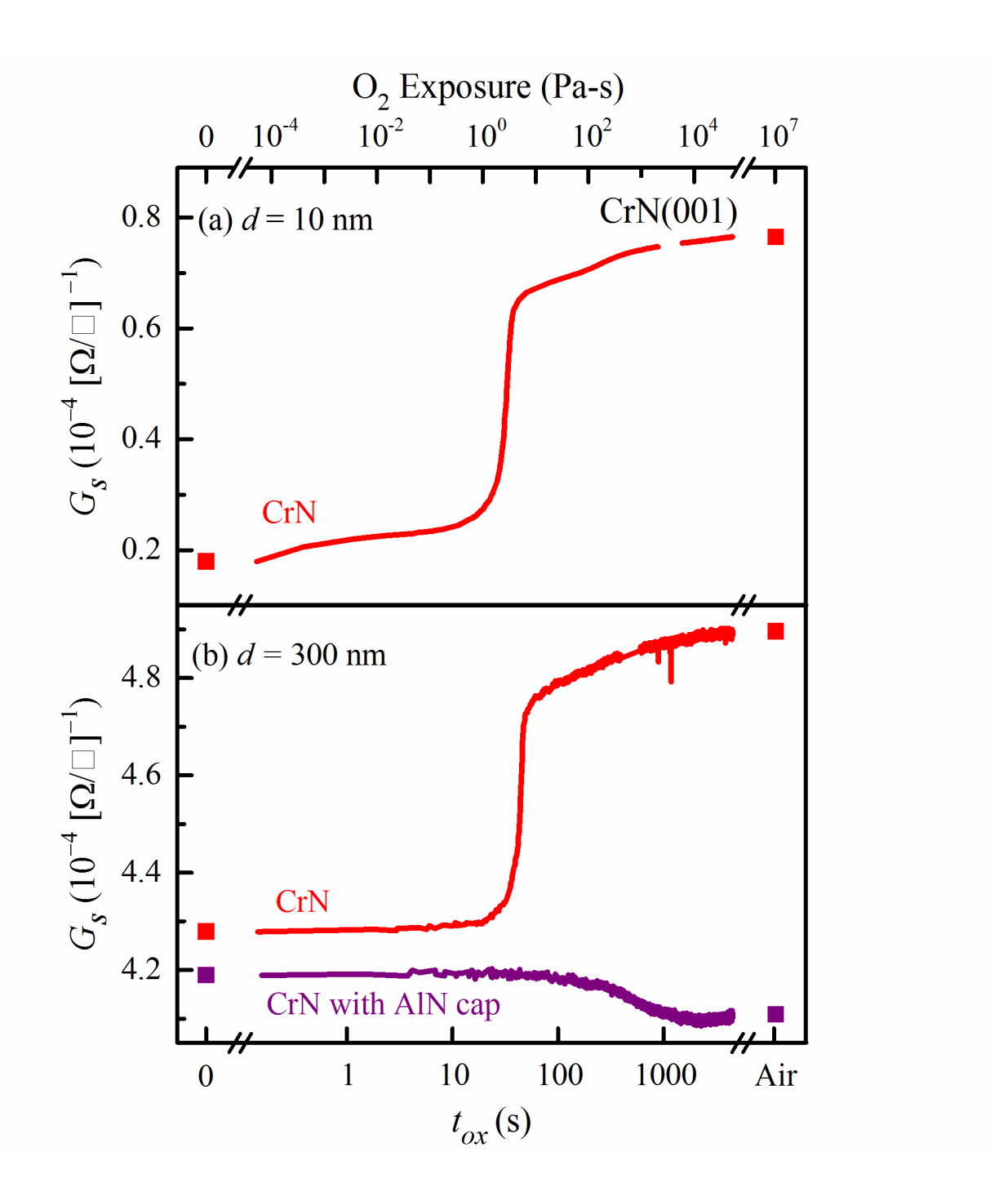


Figure 1: Measured sheet conductance  $G_s$  vs oxidation time  $t_{ox}$  (bottom axis) and  $O_2$  exposure (top axis) of epitaxial CrN(001) layers with (a) thickness d = 10 nm and (b) d = 300 nm with and without an AlN cap layer.

### References

- <sup>1</sup>X.Y. Zhang and D. Gall, Phys. Rev. B **82**, 045116 (2010).
- <sup>2</sup> A. Herwadkar and W.R.L. Lambrecht, Phys. Rev. B **79**, 035125 (2009).
- <sup>3</sup> B. Alling, T. Marten, and I.A. Abrikosov, Phys. Rev. B **82**, 184430 (2010).
- <sup>4</sup> I. Stockem, A. Bergman, A. Glensk, T. Hickel, F. Körmann, B. Grabowski, J. Neugebauer, and B. Alling, Phys. Rev. Lett. **121**, 125902 (2018).
- <sup>5</sup> P.A. Anderson, R.J. Kinsey, S.M. Durbin, A. Markwitz, V.J. Kennedy, A. Asadov, W. Gao, and R.J. Reeves, J. Appl. Phys. **98**, 043903 (2005).
- <sup>6</sup> A. Ney, R. Rajaram, S.S.P. Parkin, T. Kammermeier, and S. Dhar, Appl. Phys. Lett. **89**, 112504 (2006).
- <sup>7</sup>A. Ney, R. Rajaram, S.S.P. Parkin, T. Kammermeier, and S. Dhar, Phys. Rev. B. **76**, 03520 (2007).
- <sup>8</sup> C.X. Quintela, F. Rivadulla, and J. Rivas, Appl. Phys. Lett. **94**, 152103 (2009).
- <sup>9</sup> C.X. Quintela, B. Rodríguez-González, and F. Rivadulla, Appl. Phys. Lett. **104**, 022103 (2014).
- <sup>10</sup> C.X. Quintela, J.P. Podkaminer, M.N. Luckyanova, T.R. Paudel, E.L. Thies, D.A. Hillsberry,
- D.A. Tenne, E.Y. Tsymbal, G. Chen, C.-B. Eom, F. Rivadulla, C.X. Quintela, J.P. Podkaminer,
- C. Eom, M.N. Luckyanova, G. Chen, T.R. Paudel, E.Y. Tsymbal, E.L. Thies, D.A. Hillsberry, D.A. Tenne, and F. Rivadulla, Adv. Mater 27, 3032 (2015).
- <sup>11</sup> P. Panjan, B. Navinšek, A. Cvelbar, A. Zalar, and I. Milošev, Thin Solid Films **281–282**, 298 (1996).
- <sup>12</sup> P. Hones, C. Zakri, P.E. Schmid, F. Lévy, and O.R. Shojaei, Appl. Phys. Lett. 76, 3194 (2000).
- <sup>13</sup> I. Milošev, J.M. Abels, H. -H. Strehblow, B. Navinšek, and M. Metikoš-Hukovič, J. Vac. Sci. Technol. A Vacuum, Surfaces, Film. **14**, 2527 (1996).
- <sup>14</sup> C.P. Mulligan, T.A. Blanchet, and D. Gall, Surf. Coatings Technol. 203, 584 (2008).
- <sup>15</sup> C.P. Mulligan, T.A. Blanchet, and D. Gall, Surf. Coatings Technol. **204**, 1388 (2010).
- <sup>16</sup> C.P. Mulligan and D. Gall, Surf. Coatings Technol. **200**, 1495 (2005).
- <sup>17</sup> P. Panjan, B. Navinšek, A. Cvelbar, A. Zalar, and J. Vlcek, Surf. Coatings Technol. **98**, 1497 (1998).
- <sup>18</sup> M. Čekada, P. Panjan, B. Navinšek, and F. Cvelbar, Vacuum **52**, 461 (1999).
- <sup>19</sup> P. S. Herle, M. S. Hegde, N. Y. Vasathacharya, S. Philip, M. V. R. Rao, and T. Sripathi, J. Solid State Chem. 134, 120 (1997)
- <sup>20</sup> R. Mientus and K. Ellmer, Surf. Coatings Technol. **116–119**, 1093 (1999).
- <sup>21</sup> D. Gall, C.-S. Shin, R.T. Haasch, I. Petrov, and J.E. Greene, J. Appl. Phys. **91**, 5882 (2002).
- <sup>22</sup> C. Constantin, M.B. Haider, D. Ingram, and A.R. Smith, Appl. Phys. Lett. **85**, 6371 (2004).
- <sup>23</sup> K. Inumaru, K. Koyama, N. Imo-oka, and S. Yamanaka, Phys. Rev. B **75**, 054416 (2007).
- <sup>24</sup> J.D. Browne, P.R. Liddell, R. Street, and T. Mills, Phys. Status Solidi 1, 715 (1970).
- <sup>25</sup> Y. Tsuchiya, K. Kosuge, Y. Ikeda, T. Shigematsu, S. Yamaguchi, and N. Nakayama, Mater. Trans. JIM **37**, 121 (1996).
- <sup>26</sup> D. Gall, C.-S. Shin, T. Spila, M. Odén, M.J.H. Senna, J.E. Greene, and I. Petrov, J. Appl. Phys. **91**, 3589 (2002).
- <sup>27</sup> R. Sanjinés, O. Banakh, C. Rojas, P.. Schmid, and F. Lévy, Thin Solid Films **420–421**, 312 (2002).
- <sup>28</sup> X.Y. Zhang, J.S. Chawla, R.P. Deng, and D. Gall, Phys. Rev. B **84**, 073101 (2011).
- <sup>29</sup> X.Y. Zhang, J.S. Chawla, B.M. Howe, and D. Gall, Phys. Rev. B **83**, 165205 (2011).

- <sup>30</sup> F. Rivadulla, M. Bañobre-López, C.X. Quintela, A. Piñeiro, V. Pardo, D. Baldomir, M.A. López-Quintela, J. Rivas, C.A. Ramos, H. Salva, J.-S. Zhou, and J.B. Goodenough, Nat. Mater. **8**, 947 (2009).
- <sup>31</sup> X.F. Duan, W.B. Mi, Z.B. Guo, and H.L. Bai, J. Appl. Phys. **113**, 023701 (2013).
- <sup>32</sup> P. Tomeš, D. Logvinovich, J. Hejtmánek, M.H. Aguirre, and A. Weidenkaff, Acta Mater. **59**, 1134 (2011).
- <sup>33</sup> S. Nagasawa, K. Suzuki, A. Sato, T. Suzuki, T. Nakayama, H. Suematsu, and K. Niihara, Jpn. J. Appl. Phys. **55**, 02BC18 (2016).
- <sup>34</sup> R. Arvinte, J. Borges, R.E. Sousa, D. Munteanu, N.P. Barradas, E. Alves, F. Vaz, and L. Marques, Appl. Surf. Sci. **257**, 9120 (2011).
- <sup>35</sup> R. Mientus, R. Grötschel, and K. Ellmer, Surf. Coatings Technol. **200**, 341 (2005).
- <sup>36</sup> I. Milošev, H.-H. Strehblow, and B. Navinšek, Thin Solid Films **303**, 246 (1997).
- <sup>37</sup> I. Milošev, H.-H. Strehblow, and B. Navinšek, Surf. Coatings Technol. **74–75**, 897 (1995).
- <sup>38</sup> A. Lippitz and T. Hübert, Surf. Coatings Technol. **200**, 250 (2005).
- <sup>39</sup> H.C. Barshilia, N. Selvakumar, B. Deepthi, and K.S. Rajam, Surf. Coatings Technol. **201**, 2193 (2006).
- <sup>40</sup> J. S. Chawla, F. Zahid, H. Guo, and D. Gall, Appl. Phys. Lett. **97**, 132106 (2010).
- <sup>41</sup> P.Y. Zheng, R.P. Deng, and D. Gall, Appl. Phys. Lett. **105**, 131603 (2014).
- <sup>42</sup> J.R. Frederick and D. Gall, Appl. Phys. Lett. **87**, 053107 (2005);
- <sup>43</sup> X.Y. Zhang and D. Gall, Thin Solid Films **518**, 3813 (2010).
- <sup>44</sup> K. Zhang, K. Balasubramanian, B.D. Ozsdolay, C.P. Mulligan, S.V. Khare, W.T. Zheng, and D. Gall, Surf. Coat. Technol. **288**, 105 (2016).
- <sup>45</sup> P.Y. Zheng, B. D. Ozsdolay, and D. Gall, J. Vac. Sci. Technol. A **33**, 061505 (2015).
- <sup>46</sup> S.P. Lewis, P.B. Allen, and T. Sasaki, Phys. Rev. B **55**, 10253 (1997).